JCI insight

Comprehensive analysis of mesenchymal cells reveals a dysregulated TGF-β/Wnt/HOXB7 axis in patients with myelofibrosis

Saravanan Ganesan, … , Christine Chomienne, Bruno Cassinat

JCI Insight. 2024. https://doi.org/10.1172/jci.insight.173665.

Research In-Press Preview Hematology

Graphical abstract

Figure 6

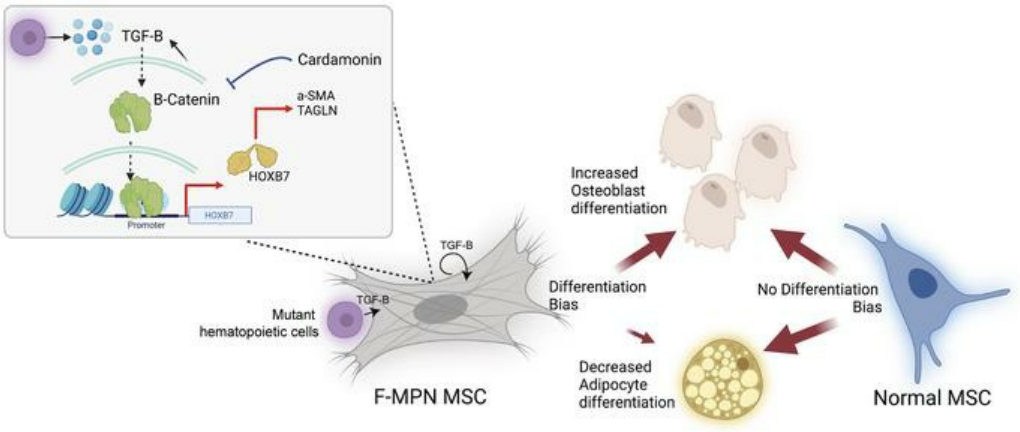

Comprehensive analysis of mesenchymal cells reveals a dysregulated TGF-β/Wnt/HOXB7 axis in patients with myelofibrosis

Saravanan Ganesan[1#], Sarah Awan-Toor[1#], Fabien Guidez[1,2], Nabih Maslah[1,3], Rifkath Rahimy[4], Céline Aoun[1], Panhong Gou[1], Chloé Guiguen[1], Juliette Soret[5], Odonchimeg Ravdan[3], Valeria Bisio[6], Nicolas Dulphy[6,7], Camille Lobry[8], Marie-Hélène Schlageter[3], Michèle Souyri[1], Stéphane Giraudier[1,3], Jean-Jacques Kiladjian[1,5], Christine Chomienne[1*] and Bruno Cassinat[1,3*]

Affiliation :

[1] INSERM UMRS 1131, Institut de Recherche Saint-Louis, Université Paris Cité, Paris F-75010, France
[2] INSERM U1232/LNC, Team Epi2THM, UBFC, Dijon, France
[3]AP-HP, Hôpital Saint-Louis, Service de Biologie Cellulaire, Paris F-75010, France
[4] Laboratoire de recherche en génétique et hématologie translationnelle, Institut Gonçalo Moniz, Salvador, Bahia, Brésil
[5] INSERM CIC 1427, Université Paris Cité, AP-HP, Hôpital Saint-Louis, Centre d'Investigations Cliniques, Paris F-75010, France
[6] INSERM UMRS 1160, Institut de Recherche Saint-Louis, Université Paris-Cité, Paris F-75010, France
[7]AP-HP, Hôpital Saint-Louis, Laboratoire d'Immunologie et d'Histocompatibilite, Paris F-75010, France
[8] INSERM U944, CNRS UMR7212, Institut de Recherche Saint Louis, Université Paris-Cité, Paris F-75010, France

[#] These authors contributed equally
* These authors contributed equally as senior authors

Correspondence to : Dr Bruno CASSINAT, Laboratoire de Biologie Cellulaire, Hopital Saint-Louis, Paris, France. Tel: +33 1 42 49 42 03. Email: bruno.cassinat@aphp.fr

The authors have declared that no conflict of interest exists

Abstract

Despite the advances in the understanding and treatment of myeloproliferative neoplasm (MPN), the disease remains incurable with the risk of evolution to AML or myelofibrosis (MF). Unfortunately, the evolution of the disease to MF still remains poorly understood impeding preventive and therapeutic options. Recent studies in solid tumor microenvironment and organ fibrosis have shed instrumental insights on their respective pathogenesis and drug resistance, yet such precise data are lacking in MPN. In this study, through a patient-sample driven transcriptomic and epigenetic description of the MF microenvironment landscape and cell-based analyses, we identify HOXB7 overexpression and more precisely a novel TGF-β-Wnt-HOXB7 pathway as associated to a pro-fibrotic and pro-osteoblastic biased differentiation of mesenchymal stromal cells (MSCs). Using gene-based and chemical inhibition of this pathway, we reverse the abnormal phenotype of MSCs from myelofibrosis patients, providing the MPN field with a potential novel target to prevent and manage evolution to MF.

Introduction

Myelofibrosis (MF) is a life-threatening complication of *BCR::ABL1* negative myeloproliferative neoplasms (MPN) induced by the MPN cell clonal proliferation, leading to bone marrow fibrosis, extra-medullary hematopoiesis and acute leukemia transformation (1). For MPN patients, this results in extremely poor quality of life and overall shortened survival (2). The progression of MPN to MF is reported with a frequency that could be as high as 10% at 10 years and 20% at 20 years (3) with an overall short median survival of 6 years when MF is established (2). So far, the knowledge gained on the MPN hematopoietic clone at the genetic and phenotypic level has provided instrumental descriptive information for MPN management but has not changed the prevention or treatment of MF. Retrospective MPN patient studies reveal that PV (Polycythemia Vera) patients homozygous or with a high allele burden for $JAK2^{V617F}$mutations are more likely to progress to MF (4) while post–essential thrombocythemia MF patients were more likely to have a high frequency of "non-driver" mutations affecting epigenetic regulation and the spliceosome machinery (ASXL1 and EZH2 mutations) (5). Recently, differential methylation of CpG sites of genes involved in cancer, embryonic development, inflammatory disease, or immunological diseases was identified in MF CD34+ cells (6). Unfortunately, no association between a single-somatic gene mutation of the MPN clone and MPN evolution to MF was identified spurring further studies to characterize alterations occurring in the microenvironment of the MPN clone.

Extensive studies in MF point to MPN mesenchymal stromal cells (MSCs) as key players. TGF-β has been shown since decades to have a direct role in fibrosis whether in MF or in other fibrotic diseases (1) and murine MF models show efficient targeting of the TGF-β receptor I (7) or TGF-β result in the reduction or inhibition of fibrosis (8). In MPN patients, other cytokines such as IL-1β , IL-8, IL-2R, IL-6, TNF-α (9), CCL2 (10), lipocalin-2 (11), oncostatin-M (12), PDGF (13),

FGF and VEGF (14), inhibitors of metallo proteinase (15) and more recently IL-13 (16) have also been associated with the establishment of MF. An overall remodeling of the local hematopoietic niche by cytokine storms such as induced by IL-1β may also contribute to fibrosis (17). Recently pro-fibrotic MSC subpopulations with increased expression of alarmins have been identified in MPN patients who progress to fibrosis (18). Thus, clear evidence exists that during MPN evolution, both the MPN clone(s) and the MPN MSCs are subject to numerous external and internal altered signals. How these signals activate which pathways leading to fibrosis needs to be further unraveled.

To contribute in the ongoing research, we designed a study to comprehensively analyze the MSCs of MF MPN patients. Leaning on a well characterized MPN patient cohort both at the pathology and genomic level, we identify ~~a novel~~ the TGF-β/Wnt/HOXB7 axis in MF patients' MSCs that is efficiently targeted in vitro.

Results

MSCs from fibrotic MPN patients have distinct signatures and are biased towards osteoblast differentiation. While expanded MSCs from MPN patients with criteria of fibrosis (19) which will be referred to as fibrotic MPN MSCs (F-MPNs, n=12) (Figure 1A, Supplemental Table1 and described in Mat Methods), presented as stellar-shaped cells in a clustered growth pattern, MSCs from age-matched (controls, n=17) showed a normal spindle shape (Figure 1B). The expansion and growth appeared slower in F-MPNs than in control MSCs, albeit at a patient-dependent level (data not shown). F-MPNs expressed well-known cell surface MSC markers (CD105, CD90,

CD73), however their level of expression differed from control MSCs with an increased CD105 expression and a decreased CD90 and CD73 expression (Figure 1C). As reported previously (20), these F-MPNs also expressed high levels of the cell-surface fibrosis marker- LEPR (CD295), but a lower than reported expression of PDGFR-α (CD140a) (Figure 1C) which may indicate hyperstimulation of the PDGFR-α by PDGF . Indeed, analysis of the cytokine profile secreted from these expanded MSCs highlighted a pro-inflammatory profile for the F-MPNs as seen through an increased secretion of pro-inflammatory cytokines such as IL-1α, IL-1β, IL-8, IL-6, CCL2, PDGF. As expected, these F-MPNs secrete high levels of TGF-β 1, TGF-β 2 and TGF-β 3, of which TGF-β 1 is a known driver of fibrosis in MPN (1) (Figure 1D). None of the F-MPNs (n= 12) stromal cells expanded expressed MPN driver mutations (Supplemental Table 1). RNA-seq analysis of these expanded F-MPNs (n = 7) equally underscored their distinct features compared to control MSCs (Control = 4) at the transcriptional level (Figure 1E) with more than 1600 differentially regulated genes (Figure 1F). F-MPNs gene expression profiles were enriched for fibrosis-associated genes (Figure 1, F and G) further validating the clinical and pathology selection criteria used for the MPN samples of this analysis (Supplemental Table I). GSEA analysis identified a dysregulation of fibrotic tissue pathways such as the TGF-β pathway, cytoskeleton regulation and NOTCH signaling (Figure 1G). Interestingly, we discovered a significant enrichment of WNT signaling and a disrupted MSC differentiation pattern with an increase of osteoblast differentiation associated genes and a decrease of adipocyte-associated genes suggesting a differentiation bias of F-MPNs (Figure 1, H and I).

To further confirm and decipher the dysregulated gene expression observed in F-MPNs, we first looked to chromatin accessibility in samples of the RNA-seq cohort (3 each for F-MPN and control MSCs). Based on differential peak calling (DESeq2 analysis), the F-MPNs showed a

distinct chromatin accessibility profile from control age-matched MSCs (Figure 2A). A further analysis, provided insights into the accessible Transcription factors (TFs) binding sites. The motif analysis (HOMER-based motif analysis) pointed to an enrichment of binding sites for TFs involved in fibrosis (Table 1). In line with the upregulation of the TGF-β pathway genes observed in these F-MPN samples, we noted an enrichment of SMAD3, RUNX2, and SP5 transcription factor motifs (Table 1). Interestingly, these TFs are associated to osteoblast differentiation (21, 22). We also noted a significant distinct enrichment of other osteoblast lineage TF motifs (23-26) such as FRA-1, ATF-3, FRA-2, AP-1, TEAD4 in F-MPN (Supplemental Figure 1). Integrating RNA-seq data and ATAC-seq data of genes involved in osteoblast lineage differentiation, clearly identified an increased accessibility of the promoters of *ACTA2* and *PLZF1* genes though other osteoblast lineage differentiation genes such as those highly expressed in the RNA-seq study (Figure 1I) or reported in the literature did not come out as significant at the time of analysis (27-30). More significantly, the CEBP/α TF motif involved in adipocyte differentiation (31) was reduced, corroborating the RNA-seq results (Supplemental Figure 2) and in line with the significant reduced chromatin accessibility for a CEBP/α target gene, *PPARγ,* a master gene of adipocyte differentiation (32). These omics data of the F-MPN MSCs differentiation capacity were validated by qRT-PCR on a larger cohort of F-MPN and control samples including samples used for RNA-seq and ATAC-seq (n=10 and 12 F-MPNs and control MSCs samples) which confirmed an increased expression of osteoblast genes (*ACTA2, PLZF1*) and decreased expression of adipocyte gene (*PPARγ*) and chondrocyte gene (*SOX9;* figure 2C). Finally, to confirm these molecular findings, we performed a functional differentiation assay of F-MPNs (n=12) and control MSCs (n=10). After 21 days of culture and using lineage specific staining (alizarin red and Oil red O respectively) F-MPNs show an increased osteo-differentiation and reduced adipocyte

differentiation (Figure 2D). Overall, the findings of this integrated transcriptome and epigenome analysis in MF MPN patients, point to an upregulation of osteoblast differentiation and fibrosis genes in the MSCs of MPN patients with fibrosis. These results are in line with previous studies (18, 33) and validate this cohort for the following studies of MF patient MSCs continued below.

TGF-β-induced HOXB7 expression promotes fibrosis and osteoblast differentiation in F-MPN MSCs. The *HOXB7* gene is one of the most significantly dysregulated genes in the top 50 dysregulated genes of the F-MPN MSCs RNA-seq study, (Figure 3A). To our knowledge this is the first time that HOXB7 is linked to MPN MSCs at any stage of the disease. ATAC-seq data corroborated this finding and showed that, in F-MPN MSCs there is an increased chromatin accessibility at the HOXB gene cluster and in particular at the *HOXB7* gene region when compared to age-matched control MSCs (Figure 3B). qRT-PCRs of the *HOXB7* gene and other HOXB genes (*HOXB2, HOXB5* and *HOXB9*) confirmed the dysregulation of a HOXB pathway in these F-MPN MSCs (Figure 3C).

Of interest for this study*, HOXB7* has already been related to the differentiation of stromal cells towards the osteoblast lineage (34). We thus questioned whether the increased expression of HOXB genes noted in the MSCs of these fibrotic MPN patients, that equally present with a biased differentiation towards osteoblast differentiation (RNA-Seq data), could be induced by the malignant MPN clone. To answer this question, we established an in vitro co-culture system where a normal human MSC cell line (HS-5) was co-cultured with a MPN human cell line UT7, bearing either a $JAK2^{V617F}$ mutant (MUT) or a wild type (WT) *JAK2* gene (Figure 3D). After 7 days of co-culture, an upregulation of the *HOXB7* gene as well as the *ACTA2* gene (fibrotic gene) was observed in HS-5 cells co-cultured with the $JAK2^{V617F}$ mutant cell line (Figure 3E). A similar differential expression was noted when HS-5 cells were cultured with conditioned media from the

WT or MUT cells (Figure 3E). Incubation of the HS-5 cells with 10ng /ml TGF-β equally induced an up-regulation of *HOXB7* and *ACTA2* genes (Figure 3E). In summary this analysis shows that in F-MPNs, *HOXB7* and fibrosis-associated genes are dysregulated and that the MPN *JAK2* mutated clone has the potential to modify their expression in normal MSCs via their secretome.

To further establish the relationship between HOXB7 and osteoblast differentiation of MPN MSCs, we generated a stable *HOXB7* knock-down (KD) HS-5 cell line using lentiviral shRNA (Figure 4A and B, supplementary Figure 4). HS-5 cells that do not express HOXB7 (HS5-HOXB7-KD3) (Figure 4A) show clear reduced chromatin accessibility and reduced gene expression for *ACTA2* and *TAGLN* genes - genes involved in fibrosis and osteoblast differentiation *(*Figure 4, C and D). A Western Blot confirms the decreased protein expression for *ACTA2* (coding for a-SMA) *(*Figure 4B). In order to establish the fact that HOXB7 is regulated by TGF-β and influences the expression of downstream genes such as *TAGLN*, we made a doxycycline inducible knock down of HOXB7 where we show that even in the presence of TGF-β, induction of the HOXB7 knock down reduces the expression of *TAGLN* (figure 4E) while restoration of HOXB7 by doxycycline withdrawal triggers a recovery of *TAGLN* expression (Figure 4E). Importantly, we also observed that in the absence of *HOXB7* gene, the differentiation profile of HS-5 MSCs showed a significant reduction in osteoblastic lineage even in the presence of TGF-β (Figure 4F). These results support the role of TGF-β-induced HOXB7 expression as a master regulator for both fibrosis and osteoblast differentiation in human MSCs from MPN patients.

Targeting WNT signaling counteracts the TGF-β-HOXB7 driven pro-fibrotic and pro-osteoblastic fate of MSCs. Because a WNT signature was noted in F-MPN MSCs RNA-seq and ATAC-seq studies (SP5 motif enrichment) (Figure 1H, Table 1), we hypothesized that a WNT signaling pathway could regulate HOXB7 expression downstream of a TGF-β signaling. Towards this, we

analyzed canonical WNT signaling features in HS-5 cells treated with TGF-β. An increased stability of β-Catenin, its translocation into the nucleus (Figure 5, A and B), and binding on the promoter of *HOXB7* gene along with a reduced H3K9me3 mark were noted upon TGF-β treatment. (Figure 5C). Furthermore, absence of β-catenin (β-catenin KD HS-5 cell line) leads to a reduced expression of not only HOXB7 protein but also of the fibrosis-associated α-SMA protein (product of the *ACTA2* gene) (Figure 5D). A differentiation assay further shows a decreased osteoblast differentiation and increased adipocyte differentiation of the β-catenin KD HS-5 cell line (Figure 5E). All together, these data show that in MSCs, WNT signaling, when activated by TGF-β, controls the expression of HOXB7 leading to a bias towards osteoblast differentiation and possibly to fibrosis as suggested by the increased ACTA2/α-SMA expression.

As lentiviral triggered absence of β-catenin restored the differentiation bias, we next tested whether chemical inhibitors of WNT signaling could target this novel axis of HOXB7 activation in MSCs. Treatment of HS-5 cells with an inhibitor of WNT signaling (Cardamonin – 20uM) was effective to decrease protein levels of WNT targets (Cyclin D1 and C-MYC) but also to reduce TGF-β-induced *HOXB7* expression (Figure 5F). Of note, the expression of HOXB7 was not modified by the JAK1/2 inhibitor ruxolitinib frequently used to treat MPN patients (supplementary Figure 5). The inhibition of WNT signaling equally decreased the expression of osteoblast and fibrosis associated genes (Figure 5G). Finally, in the differentiation assay, treatment of HS-5 cells with Cardamonin corrected the differentiation bias towards osteoblast, as the increased osteoblast differentiation induced by TGF-β (Figure 5H). Thus, our work identifies a TGF-β/β-catenin/HOXB7 axis, which plays an important role in pro-fibrotic features in MPN (Figure 6).

Discussion

Though an increased burst in the understanding of MPN onset has been gathered in the recent years since the identification of the *JAK2* (and others) mutations, scarce input has been gathered from the few mice models and patient studies to gain further insights in the evolution of the disease to myelofibrosis. All studies converge to support the role of patient MSCs and their modification by the MPN hematopoietic clone to trigger myelofibrosis. The cytokine release by the MPN clone remains still the main constant triggering mechanism where TGF-β is the main player. Fine-tuning of the various MSCs populations, cytokines and adhesion molecules continues to complete the MPN fibrosis landscape. However, few descriptions of the genetic and epigenetic alterations of MF MPN MSCs are available maybe due to the difficulties of cell sampling for these studies whether in MF patients or mice models, impeding the discovery of preventive or therapeutic options.

To fill this gap of knowledge, we leaned on a substantial well-established and characterized MPN-MF patient cohort of our center and designed an approved study to perform biopsies in MPN-MF patients to comprehensively analyze the in vitro expanded fibrotic MSCs from MPN patients using multi-omics techniques. The data from the analysis of this cohort of MPN-MF patients' MSCs showed all the characteristics previously reported for MPN fibrosis at the molecular and gene expression level, whether in cell surface markers, cytokine secretion, biased differentiation towards the osteoblast lineage, fibrosis gene expression profile including WNT altered pathways (1, 18, 20, 33). The role of WNT signaling in MSC osteoblast lineage commitment is very well understood (35, 36) as its crosstalk with other differentiation pathways (37), however how these pathways act together to induce pathologic differentiation is not clearly understood.

This unique well-characterized and validated MPN-MF patients MSC cohort, allows to give strong credit to the identification of a novel candidate pathway, the HOXB cluster, in the top50 dysregulated genes. ATAC-seq data confirmed an indeed significant accessibility in *HOXB* family of genes including *HOXB7* and its close neighbor *HOXB9,* but also *HOXB2, HOXB5* and *HOXB-AS3.* The role of HOXB in skeletal regeneration and MSC differentiation is known (38, 39). Interestingly, the most highly expressed gene in this study is the *HOXB7* gene, equally known in the field of MSCs and osteoblast differentiation but never identified until now in the field of MPN. The role of *HOXB7* in MPN MSC osteoblast differentiation was confirmed, when inhibition of *HOXB7* expression and not HOXB9 expression in MSCs-induced differentiation, decreased osteoblast differentiation. The decreased osteoblast differentiation persisted even in the presence of TGF-β in line with the MSC HOXB code (40). Leaning on the robust co-culture system of normal MSC cell line with a mutant JAK2 human MPN cell line, we established that the *HOXB7* gene was controlled by the interaction of the MSC with the mutant MPN clone. This control was further shown mediated by the malignant clone's secretome and TGF-β known as the major player in the secretome. We also noted that the expanded fibrotic MSCs produced inflammatory cytokines including TGF-β suggesting that fibrotic MSCs are also capable of inducing autocrine TGF-β signaling. These results clearly substantiate the role of the interaction with the MPN clone and/or autocrine TGF-β in the upregulation of HOXB7 in MPN MSCs, and the subsequent biased differentiation towards the osteoblast lineage.

As both TGF-β and Wnt signaling pathways were dysregulated in the MPN MSCs RNA-seq and ATAC-seq data, we designed in vitro studies to unravel the molecular actors of TGF-β /Wnt signaling in MPN MSCs. We highlighted an activation of the canonical WNT pathway upon TGF-β treatment of MSCs, and most interestingly a binding of β-catenin to the promoter of

HOXB7. Such a crosstalk between TGF-β and Wnt signaling has previously been reported (41), but for the first time, we identify that this signaling is necessary for *HOXB7* activation. We further confirmed the existence of this TGF-β/WNT/HOXB7 axis when a reduced osteoblast differentiation and *ACTA2* gene expression resulted from the inhibition of β-Catenin.

Thus, in MPN MSCs there exists a crosstalk between TGF-β/WNT and HOXB7 that induces osteoblast differentiation. Although, one study on primary and secondary MF patients highlighted an increase in β-catenin mRNA in the bone marrow mononuclear cells (42), to our knowledge Wnt/β-catenin upregulation in F-MPN MSC has never been previously reported. This data also provides further impact on the already well described role of TGF-β in fibrosis and in MPN fibrosis. We confirm that TGF-β was attributed to the hematopoietic mutant clone of MPN, as co-culture studies with cell-cell contacts or mutant clone conditioned media produced similar results as incubation with TGF-β alone. However, we cannot eliminate the possibility of autocrine TGF-β signaling in a fibrotic setting. This data stresses once more the role of the mutated clone in mediating MPN progression to MF, whether directly or by modification of the MPN MSC and microenvironment ,data further corroborated by the fact that the MSCs of this study did not carry any known MPN driver mutation. Other mechanisms may occur in vivo as noted in a mouse model in which neuropathy may induce MSC alterations leading to fibrosis in MPN (17), in vivo results partially confirmed in a clinical trial (43).

In summary, we demonstrate that the biased osteoblast differentiation of fibrotic MSCs is mediated by the MPN hematopoietic mutated clone and its secretion of TGF-β. Our study attributes this bias to the dysregulation of the MSCs *HOXB7* gene by a TGF-β induced WNT signaling. Thus, ~~for the first time,~~ a deregulated TGF-β/WNT/HOXB7 axis pathway is identified

in MPN-MF evolution offering a potential monitoring and therapeutic target for MPN patients with MF.

Methods

Sex as a biological variable. In this study both male and female patients were included. Sex of patients was not considered as a biological variable.

Human MPN primary cells and cell lines. Bone marrow samples and biopsies from MPN patients were collected for diagnostic purposes and mesenchymal stromal cells were isolated after obtaining written informed consent. The human UT-7 Megakaryoblastic cell line lentivirally transduced with wild-type JAK2 or JAK2V617F mutated gene, HS-5 cell lines (obtained from ATCC, USA) and HS-5 B-Cat KD line (Kind gift from Dr. Vikram Mathews, CMC Vellore, India) were also used in this study.

Mesenchymal stromal cells (MSC) expansion and differentiation. F-MPN MSCs and normal MSCs were expanded from the bone marrow biopsies from MPN patients and age-matched normal patients who underwent hip replacement surgery respectively. MSCs were cultured using MEM alpha medium (Life Technologies Inc.) with 10% fetal bovine serum (Life Technologies Inc.,), 100 units/mL penicillin and 100 ug/mL streptomycin, L-Glutamine, β- mercaptoethanol (Life technologies Inc.) in a humidified atmosphere with 5% CO2. Medium was changed every 3 days until the stroma is expanded. Stromal cells from passage 2 or 3 were used for the study. For osteoblast and adipocyte differentiation, the MSCs from passage 2 were used. The medium for osteoblast differentiation was MEM alpha (Life technologies Inc.) supplemented with 10% FBS, pen-strep (1%), L-glutamine (1%), Dexamethasone (0.1uM), β-Glycerophosphate (10mM), Ascorbic acid (50uM). The medium for adipocyte differentiation was low glucose DMEM (Life

technologies Inc.) with 10% FBS, pen-strep, L-glutamine, 3- Isobutyl-1- methylxanthine (0.5mM), Indomethacin (60uM), Insulin (100ng/ml) and hydroxycortisone (0.5uM). In either osteoblast or adipocyte differentiation assays cells were cultured for 21 days with replacement of differentiation media every 3 days. The osteoblast and adipocyte differentiation were confirmed using alizarin red S staining and Oil Red O staining respectively.

Cytokines and inhibitors. Cardamonin was purchased from Merck, TGF-β1 from Biotechne and ruxolitinib from MedChemExpress. All molecules were reconstituted and stored according to the suppliers instructions.

Lentivirus mediated knockdown. The shRNAs for scramble and *HOXB7* were purchased from Sigma (TRC cloning vectors - Sigma, St.Louis, MO, USA). The plasmids were amplified, and lentiviral particles were generated according to standard protocols. The efficacy of transduction was measured through GFP positive cells which acted as a positive control. The lentiviral particles generated were used to transduce HS-5 cells for 6 hours and the medium was changed, allowing the cells to grow in complete media for 24 hours. The transduced cells were selected with puromycin (1mg/mL) for 2 weeks and the knockdown was confirmed by western blot assays.

Quantitative real-time PCR. Total RNA was extracted using Trizol reagent (Invitrogen Carlsbad, CA, USA). 500ng of the extracted RNA was converted into cDNA using a superscript III cDNA kit (Invitrogen Carlsbad, CA, USA). The expression of genes was studied using the SYBR green method (Applied Biosystems, Thermofischer scientific, USA) (primer sequence used were given in reagents section). The Ct values were normalized with *ACTB* and the fold differences were calculated using the $2^{-\Delta Ct}$ method or $2^{-\Delta\Delta Ct}$.

RNASeq Experiments. RNAseq was performed at Plateforme de Génomique Institut Cochin Inserm 1016-CNRS, Paris, France. Total RNA libraries were prepared using the Illumina TruSeq

RNA kit as described by the manufacturer (Illumina). 1 microgram of total RNA was used from each sample for the library preparation. 5` and 3` RNA adaptors were ligated to the RNA and the ligated products were reverse transcribed using superscript II reverse transcriptase (Invitrogen). The size and integrity of each library were verified using the Bioanalyser (Agilent). The libraries were sequenced on an Hiseq 1000 instrument (Illumina). The differentially expressed RNA was analyzed using DESeq with an FDR corrected p values < 0.05. Briefly, reference-based de novo transcriptome assembly was performed using Cufflinks (version 0.9.3) and Scripture. RefSeq and Ensemble annotated transcripts were filtered out from Scripture and Cufflinks assembled transcriptomes. De novo transcript assembly was processed through Trinity and the CPC scores were determined. To determine the number of statistically significant differentially expressed RNA for hierarchical clustering, SAMseq was performed and significant transcripts with FDR < 0.05 were identified.

ATAC-seq experiment. The ATAC-seq on MSCs was carried out by Active motif inc (USA). In short, 50k viable nuclei were tagmented using Tn5 enzyme pre-loaded with next-gen sequencing adapters, followed by amplification of tagmented DNA using standard primers from the kit (Active -motif inc, USA). The amplified libraries were subjected to sequencing using Hiseq500 (Illumina). The paired-end 42 bp sequencing reads (PE42) generated are mapped to the genome using the BWA algorithm. Genomic regions with high levels of transposition/tagging events are determined using the MACS2 peak calling algorithm and the fragment density was determined followed by normalization of the reads. After identifying merged regions as part of the standard analysis pipeline, the DESeq2 software is run on the unnormalized BAM files (without duplicates). We then perform HOMER motif analysis (findMotifsGenome.pl) on the 200 bp sequence centered

around the midpoint of the differential region (+100 bp, -100 bp) to identify transcription factor motifs.

Immunoblots. HS-5 cells were harvested and the pellets were lysed in RIPA buffer (Sigma, St.Louis, MO, USA) for 30 minutes in ice, with complete protease inhibitors (Roche, Basel, Switzerland). The lysates were collected by centrifugation at 13000 rpm for 10 minutes. The lysates were analyzed in SDS–PAGE. After protein transfer to a nitrocellulose membrane (BioRad, CA, USA), membranes were blocked with non-fat dry milk (5%, 2 hours at room temperature) followed by incubation with primary antibodies overnight at 4 degrees Celsius. The protein bands were detected by the standard chemiluminescence method (Thermo Pierce Femto, Rockford, IL, USA). For imaging, an ImageQuant system (Amersham) was used.

Chromatin Immunoprecipitation (ChIP) assay. ChIP assay was performed through standard kit protocol (Digenode inc, CA USA). Antibodies against B-Catenin (SC, USA) and H3K9me3 (Digenode inc, CA, USA). The antibody bound DNA were analysed using Q-PCR using the following primers for HOXB7 promoters – Forward(5'-3') - GGGAATCACGTGCTTTTGTT and Reverse(5'-3') – TGTTTCTCCCCCTTCTCCTT.

Generation of Tet inducible HoxB7 knock down clone:

Doxycycline inducible HOXB7 shRNA were generated using Tet-pLKO-puro plasmid - a gift from Dmitri Wiederschain (Addgene plasmid # 21915 ; http://n2t.net/addgene:21915 ; RRID:Addgene_21915). The HOXB7 shRNA sequences (KD3 & KD5) from previous validated experiments were cloned according to previous reports (44). Pre-cloned scramble shRNA [Tet-pLKO-puro-Scrambled -a gift from Charles Rudin (Addgene plasmid # 47541 ; http://n2t.net/addgene:47541 ; RRID:Addgene_47541)] was used as control for the experiment. The cloned shRNA in plasmids were confirmed and were expanded in Stbl3 strain of *E.Coli*

according to the supplier's instructions (Invitrogen^{TM}). For packaging the plasmids, Pax2 and VSVG plasmids were used according to a standard protocol. 293T cells were infected in the presence of 5µg/mL polybrene and the supernatant containing viral particles was collected at 48 hours. It was filtered and concentrated overnight at 4°C using Retro-X virus concentrator (Takara Bio). The concentrated virus was spun and stored at -80°C. The virus was titrated on HS-5 cell line by overnight transduction. The next day, the medium was changed and puromycin selection (starting from 1 ug/mL and increasing to 3 ug/mL maximum) was started 2 days after transduction. After one week, the cells resistant to puromycin were dissociated and counted to determine the efficiency of transduction. The viral titer was determined and used for transducing HS-5 cells with Tet inducible scrambled and HoxB7 specific plasmids. After transduction, cells were cultured in medium containing tetracyclin-free fetal bovine serum(Takara Bio). Transduced cells were selected as already described. For inducing the sh RNA, doxycycline (Sigma) was used. Doses up to 100 ng/mL were tested and validated by qRTPCR. For experiments, a dose of 10 ng/mL was validated and used for further experiments. For experiments, the cells post exposure to doxycycline (10 ng/mL ; for 3 days) were washed in PBS and re-introduced with fresh media for another 3 days without doxycycline. RNA samples were extracted at day 0 (pre dox), day3 (post dox) and day6 (dox withdrawal) and the expression of HOXB7 and TAGLN were analyzed as described above.

Cytokines measurement. MSCs were seeded at a density of 10^6 per 75 cm² flask. Next day, the medium was changed to MEM alpha containing 2% fetal bovine serum. After 48 hours, the supernatant was spun at 3000 rpm and filtered using a 0.2-micron filter, then stored at -80°C. A custom Luminex assay was purchased from R&D systems with the following cytokines: CCL2, HGF, IGFBP-2, IL-1α, IL-Iβ, IL-6, IL-8, IL-15, leptin, lipocalin-2, PDGF isoforms AA, BB, CC and DD, thrombopoietin and VEGF. For the assay, the manufacturer's instructions were followed

and reading was done on a Biorad MAGPIX analyzer. For measuring TGF beta 1, 2 and 3, the TGF beta 3-plex assay was purchased from Biorad. As per the manufacturer's instructions, the samples were activated before incubation with the magnetic beads. A t-test was used for statistical analysis.

Quantification and statistical analysis. Statistical analyses for evaluating differences between two groups were performed using the unpaired and two-tailed Student's t test. For evaluating significance in more than two groups one way ANNOVA was used. GraphPad Prism 9 was used for these statistical analyses.

Study approval. The study was approved by the institutional review board « Comité d'Evaluation de l'Ethique des Projets de Recherche Biomédicale (CEERB) du Groupe Hospitalier Universitaire Nord de l'Assistance Publique-Hôpitaux de Paris » (IRB00006477, CER-2020-55).

Data Availability. The RNA-seq and ATAC-seq processed data have been deposited in GEO (GSE234388, GSE234389, GSE234390). Supporting data values are available in supplementary section.

Acknowledgements

This work was supported by Fondation de France (00088498/2019-20). S Ganesan was supported by an early career award from Fondation de France. We thank Romuald Peux for technical help in cytokines measurements.

Author Contributions

S. Ganesan., S. Giraudier, J.J.K., C.C. and B.C. conceived and designed the study. S.Ganesan performed most of the experiments, analysed the data and wrote the manuscript. S.A.T. designed and performed several experiments (cytokine measurements, cell culture experiments, inhibitor testing), analysed data and edited the manuscript. F.G, N.M. and C.L. analysed RNA-seq and ATAC-seq experiments. L.R., C.A., P.G., C.G. performed cell culture experiments. V.B., N.D., M.H.S. and M.S. helped with most experiments and analysis. S. Giraudier, J.S. and J.J.K. collected essential patients' specimen. C.C. and B.C supervised the work and wrote the manuscript. All authors read and edited the manuscript.

References

1. Zahr AA, Salama ME, Carreau N, Tremblay D, Verstovsek S, Mesa R, et al. Bone marrow fibrosis in myelofibrosis: pathogenesis, prognosis and targeted strategies. *Haematologica.* 2016;101(6):660-71.
2. Mughal TI, Vaddi K, Sarlis NJ, and Verstovsek S. Myelofibrosis-associated complications: pathogenesis, clinical manifestations, and effects on outcomes. *Int J Gen Med.* 2014;7:89-101.
3. Passamonti F, Giorgino T, Mora B, Guglielmelli P, Rumi E, Maffioli M, et al. A clinical-molecular prognostic model to predict survival in patients with post polycythemia vera and post essential thrombocythemia myelofibrosis. *Leukemia.* 2017;31(12):2726-31.
4. Cerquozzi S, and Tefferi A. Blast transformation and fibrotic progression in polycythemia vera and essential thrombocythemia: a literature review of incidence and risk factors. *Blood Cancer J.* 2015;5:e366.
5. Shammo JM, and Stein BL. Mutations in MPNs: prognostic implications, window to biology, and impact on treatment decisions. *Hematology Am Soc Hematol Educ Program.* 2016;2016(1):552-60.
6. Nielsen HM, Andersen CL, Westman M, Kristensen LS, Asmar F, Kruse TA, et al. Epigenetic changes in myelofibrosis: Distinct methylation changes in the myeloid compartments and in cases with ASXL1 mutations. *Sci Rep.* 2017;7(1):6774.
7. Yue L, Bartenstein M, Zhao W, Ho WT, Han Y, Murdun C, Mailloux AW, Zhang L, Wang X, Budhathoki A, Pradhan K, Rapaport F, Wang H, Shao Z, Ren X, Steidl U, Levine RL, Zhao ZJ, Verma A, Epling-Burnette PK. Efficacy of ALK5 inhibition in myelofibrosis. JCI Insight. 2017 Apr 6;2(7):e90932.

8. Gastinne T, Vigant F, Lavenu-Bombled C, Wagner-Ballon O, Tulliez M, Chagraoui H, Villeval JL, Lacout C, Perricaudet M, Vainchenker W, Benihoud K, Giraudier S. Adenoviral-mediated TGF-beta1 inhibition in a mouse model of myelofibrosis inhibit bone marrow fibrosis development. Exp Hematol. 2007 Jan;35(1):64-74.
9. Tefferi A, Vaidya R, Caramazza D, Finke C, Lasho T, Pardanani A. Circulating interleukin (IL)-8, IL-2R, IL-12, and IL-15 levels are independently prognostic in primary myelofibrosis: a comprehensive cytokine profiling study. J Clin Oncol. 2011 Apr 1;29(10):1356-63.
10. Hodeib H, Abd El Hai D, Tawfik MA, Allam AA, Selim A, Elsawy AA, Youssef A. CCL2 rs1024611Gene Polymorphism in Philadelphia-Negative Myeloproliferative Neoplasms. Genes (Basel). 2022 Mar 10;13(3):492.
11. Lu M, Xia L, Liu YC, Hochman T, Bizzari L, Aruch D, Lew J, Weinberg R, Goldberg JD, Hoffman R. Lipocalin produced by myelofibrosis cells affects the fate of both hematopoietic and marrow microenvironmental cells. Blood. 2015 Aug 20;126(8):972-82.
12. Hoermann G, Cerny-Reiterer S, Herrmann H, Blatt K, Bilban M, Gisslinger H, Gisslinger B, Müllauer L, Kralovics R, Mannhalter C, Valent P, Mayerhofer M. Identification of oncostatin M as a JAK2 V617F-dependent amplifier of cytokine production and bone marrow remodeling in myeloproliferative neoplasms. FASEB J. 2012 Feb;26(2):894-906.
13. Pourcelot E, Trocme C, Mondet J, Bailly S, Toussaint B, Mossuz P. Cytokine profiles in polycythemia vera and essential thrombocythemia patients: clinical implications. Exp Hematol. 2014 May;42(5):360-8.
14. Vaidya R, Gangat N, Jimma T, Finke CM, Lasho TL, Pardanani A, Tefferi A. Plasma cytokines in polycythemia vera: phenotypic correlates, prognostic relevance, and comparison with myelofibrosis. Am J Hematol. 2012 Nov;87(11):1003-5.
15. Bock O, Neuse J, Hussein K, Brakensiek K, Buesche G, Buhr T, Wiese B, Kreipe H. Aberrant collagenase expression in chronic idiopathic myelofibrosis is related to the stage of disease but not to the JAK2 mutation status. Am J Pathol. 2006 Aug;169(2):471-81.
16. Melo-Cardenas J, Bezavada L, Crawford JC, Gurbuxani S, Cotton A, Kang G, Gossett J, Marinaccio C, Weinberg R, Hoffman R, Migliaccio AR, Zheng Y, Derecka M, Rinaldi CR, Crispino JD. IL-13/IL-4 signaling contributes to fibrotic progression of the myeloproliferative neoplasms. Blood. 2022 Dec 29;140(26):2805-2817.
17. Arranz L, Sanchez-Aguilera A, Martin-Perez D, Isern J, Langa X, Tzankov A, et al. Neuropathy of haematopoietic stem cell niche is essential for myeloproliferative neoplasms. *Nature.* 2014;512(7512):78-81.
18. Leimkuhler NB, Gleitz HFE, Ronghui L, Snoeren IAM, Fuchs SNR, Nagai JS, et al. Heterogeneous bone-marrow stromal progenitors drive myelofibrosis via a druggable alarmin axis. *Cell Stem Cell.* 2021;28(4):637-52 e8.
19. Barbui T, Thiele J, Gisslinger H, Kvasnicka HM, Vannucchi AM, Guglielmelli P, et al. The 2016 WHO classification and diagnostic criteria for myeloproliferative neoplasms: document summary and in-depth discussion. *Blood Cancer J.* 2018;8(2):15.

20. Schneider RK, Mullally A, Dugourd A, Peisker F, Hoogenboezem R, Van Strien PMH, et al. Gli1+ Mesenchymal Stromal Cells Are a Key Driver of Bone Marrow Fibrosis and an Important Cellular Therapeutic Target. *Cell stem cell.* 2017;20(6):785-800 e8.
21. Lin HT, Chen SK, Guo JW, Su IC, Huang CJ, Chien CC, et al. Dynamic expression of SMAD3 is critical in osteoblast differentiation of PDMCs. *Int J Mol Med.* 2019;43(2):1085-93.
22. Saito H, Gasser A, Bolamperti S, Maeda M, Matthies L, Jähn K, et al. TG-interacting factor 1 (Tgif1)-deficiency attenuates bone remodeling and blunts the anabolic response to parathyroid hormone. *Nature Communications.* 2019;10(1):1354.
23. Eferl R, Hoebertz A, Schilling AF, Rath M, Karreth F, Kenner L, et al. The Fos-related antigen Fra-1 is an activator of bone matrix formation. *Embo j.* 2004;23(14):2789-99.
24. Kim JH, Kim K, Kim I, Seong S, Koh JT, and Kim N. The ATF3-OPG Axis Contributes to Bone Formation by Regulating the Differentiation of Osteoclasts, Osteoblasts, and Adipocytes. *Int J Mol Sci.* 2022;23(7).
25. Luther J, Ubieta K, Hannemann N, Jimenez M, Garcia M, Zech C, et al. Fra-2/AP-1 controls adipocyte differentiation and survival by regulating PPARγ and hypoxia. *Cell Death Differ.* 2014;21(4):655-64.
26. Zhang W, Xu J, Li J, Guo T, Jiang D, Feng X, et al. The TEA domain family transcription factor TEAD4 represses murine adipogenesis by recruiting the cofactors VGLL4 and CtBP2 into a transcriptional complex. *J Biol Chem.* 2018;293(44):17119-34.
27. Hayashi Y, Kawabata KC, Tanaka Y, Uehara Y, Mabuchi Y, Murakami K, et al. MDS cells impair osteolineage differentiation of MSCs via extracellular vesicles to suppress normal hematopoiesis. *Cell Rep.* 2022;39(6):110805.
28. Komori T. Regulation of osteoblast differentiation by Runx2. *Adv Exp Med Biol.* 2010;658:43-9.
29. Jafary F, Hanachi P, and Gorjipour K. Osteoblast Differentiation on Collagen Scaffold with Immobilized Alkaline Phosphatase. *Int J Organ Transplant Med.* 2017;8(4):195-202.
30. Lv H, Wang T, Zhai S, Hou Z, and Chen S. Dynamic transcriptome changes during osteogenic differentiation of bone marrow-derived mesenchymal stem cells isolated from chicken. *Frontiers in Cell and Developmental Biology.* 2022;10.
31. Rosen ED, Hsu CH, Wang X, Sakai S, Freeman MW, Gonzalez FJ, et al. C/EBPalpha induces adipogenesis through PPARgamma: a unified pathway. *Genes Dev.* 2002;16(1):22-6.
32. Aprile M, Ambrosio MR, D'Esposito V, Beguinot F, Formisano P, Costa V, et al. PPARG in Human Adipogenesis: Differential Contribution of Canonical Transcripts and Dominant Negative Isoforms. *PPAR Res.* 2014;2014:537865.
33. Martinaud C, Desterke C, Konopacki J, Pieri L, Torossian F, Golub R, et al. Osteogenic Potential of Mesenchymal Stromal Cells Contributes to Primary Myelofibrosis. *Cancer Res.* 2015;75(22):4753-65.
34. Gao RT, Zhan LP, Meng C, Zhang N, Chang SM, Yao R, et al. Homeobox B7 promotes the osteogenic differentiation potential of mesenchymal stem cells by activating RUNX2 and transcript of BSP. *Int J Clin Exp Med.* 2015;8(7):10459-70.
35. Houschyar KS, Tapking C, Borrelli MR, Popp D, Duscher D, Maan ZN, et al. Wnt Pathway in Bone Repair and Regeneration – What Do We Know So Far. *Frontiers in Cell and Developmental Biology.* 2019;6.

36. Kobayashi Y, Maeda K, and Takahashi N. Roles of Wnt signaling in bone formation and resorption. *Japanese Dental Science Review.* 2008;44(1):76-82.
37. Vlashi R, Zhang X, Wu M, and Chen G. Wnt signaling: Essential roles in osteoblast differentiation, bone metabolism and therapeutic implications for bone and skeletal disorders. *Genes & Diseases.* 2022.
38. Rux DR, and Wellik DM. Hox genes in the adult skeleton: Novel functions beyond embryonic development. *Dev Dyn.* 2017;246(4):310-7.
39. Seifert A, Werheid DF, Knapp SM, and Tobiasch E. Role of Hox genes in stem cell differentiation. *World J Stem Cells.* 2015;7(3):583-95.
40. Steens J, and Klein D. HOX genes in stem cells: Maintaining cellular identity and regulation of differentiation. *Frontiers in Cell and Developmental Biology.* 2022;10.
41. Jian H, Shen X, Liu I, Semenov M, He X, and Wang XF. Smad3-dependent nuclear translocation of beta-catenin is required for TGF-beta1-induced proliferation of bone marrow-derived adult human mesenchymal stem cells. *Genes Dev.* 2006;20(6):666-74.
42. Lucijanic M, Livun A, Tomasovic-Loncaric C, Stoos-Veic T, Pejsa V, Jaksic O, et al. Canonical Wnt/β-Catenin Signaling Pathway Is Dysregulated in Patients with Primary and Secondary Myelofibrosis. *Clin Lymphoma Myeloma Leuk.* 2016;16(9):523-6.
43. Drexler B, Passweg JR, Tzankov A, Bigler M, Theocharides AP, Cantoni N, et al. The sympathomimetic agonist mirabegron did not lower JAK2-V617F allele burden, but restored nestin-positive cells and reduced reticulin fibrosis in patients with myeloproliferative neoplasms: results of phase II study SAKK 33/14. *Haematologica*. 2019;104(4):710-6.
44. Wiederschain D, Wee S, Chen L, Loo A, Yang G, Huang A, et al. Single-vector inducible lentiviral RNAi system for oncology target validation. *Cell Cycle*. 2009;8(3):498-504.

FIGURE LEGENDS

Figure 1: Expanded bone marrow MSCs from F-MPN patients show an inflammatory profile and a biased osteoblast differentiation. (**A**) ~~Overall~~ experimental workflow of this study (**Illustration created using BioRender)**. (**B**) Representative phase contrast images of expanded bone marrow MSCs from either F-MPN patients ~~(F-MPNs)~~ or normal age-matched controls ~~(control MSC)~~. The spindle shape morphology of control MSCs (left) shifts to a stellar morphology in F-MPNs (right). Pictures were taken on passage 2 ~~under a regular microscope~~. Scale bar = 20x magnification. (**C**) Immunophenotypic characterization of expanded F-MPNs and control MSCs. All markers were present but differentially expressed in F-MPNs compared to controls. P-values (*- 0.05, **<0.01, ***<0.001) were calculated using unpaired t test. (**D**) Cytokine secretion profile of expanded MSCs. Day 3 supernatants at passage 2 were analyzed using a multiplexed Luminex© assay. F-MPNs show a significant increase in inflammatory cytokine levels. P-values (*- 0.05, **<0.01, ***<0.001) were calculated using unpaired t test. (**E**) Heat map and unsupervised hierarchical clustering by sample and gene were performed

using the 300 genes (RNA-Seq data) that had the largest coefficients of variation based on DESEQ2 analysis. The data are based on samples from the F-MPNs (n= 7) and control (n=4) MSC groups. (**F**) Volcano plot showing the relationship between the p-values and the log2 fold change in normalized expression (DESEQ2) between F-MPNs (n=7) and control MSCs (n=4). Genes found to be the most differentially expressed are shown in the plot by p-value. (**G**) Gene Set Enrichment Analysis (GSEA) of RNA-seq data between F-MPNs (n = 7) and control MSCs (n = 4) demonstrates an enrichment of gene sets of the fibrosis pathway. (**H**) Bargraph showing the ~~signaling~~ pathways differentially expressed in the RNA-seq analysis from control MSCs versus F-MPNs identified by DAVID Pathway Analysis. (**I**) Bargraph showing upregulation of osteoblast-associated genes and downregulation of adipocyte-associated genes in RNA-seq data of F-MPNs.

Figure 2: ATAC-seq and in vitro differentiation assays confirm the osteoblast bias of F-MPN MSCs. (**A**) Heatmap of ATAC-seq peak intensity shows different accessible chromatin regions of top 200 most variable genes (accessible chromatin – rows) across F-MPN (n=3) and control MSCs (n=3) (Columns). The color indicates scaled accessibility score. (~~**B**) HOMER DNA-motif enrichment analyses of differentially accessible peaks (F-MPN versus control) shows the enrichment of binding motifs for osteoblast differentiation transcription factors. p-value and percent of targets are given.~~ (**B**) Genome tracks around the loci of genes involved in fibrosis (*ACTA2*), osteoblast differentiation (*PLZF*), chondrocyte differentiation (*SOX9)* or adipocyte differentiation (*PPARG*) show an increased accessibility for the *ACTA2* and *PLZF* gene and a decreased accessibility for *SOX9* and *PPARG* genes in F-MPN. The genome tracks are from representative F-MPN (n=3) and control (n=3) MSCs. (**C**) qRT-PCR validation of the ATAC-seq and RNA-seq findings in F-MPN (n=10) and control MSCs (n=13). Both the fibrotic (*ACTA2*) and osteoblast markers (*PLZF*) are confirmed as up-regulated in F-MPN samples while chondrocyte or adipocyte differentiation markers (*SOX9, PPARG*) are either also confirmed as significantly decreased or at least show a trend towards significance. P-values (*- 0.05, ns- not significant) were calculated using unpaired t test. (**D**) Representative differentiation induction profile of expanded MSCs (left panel: microscopy images after respective lineage staining for osteoblastic and adipocyte lineage; right panel: arbitrary quantification of osteoblast and adipocyte differentiation). F-MPN MSCs show a biased differentiation profile towards the osteoblast lineage with a decrease in adipocyte lineage. (p-value ** <0.01) calculated using unpaired t test. Of note F-MPN-1, 2, 3, control 1, 2 3 are the same patients that we analysed in figure 1 and 3.

Figure 3: ATAQ-seq, RNAseq and co-culture studies highlight *HOXB7* upregulation in F-MPN samples. (**A**) Heat map showing the top 50 differentially regulated genes from RNA-seq data. Unsupervised hierarchical clustering by sample and gene were performed. The data are based on samples from the F-MPN (n= 7) and control (n=4) MSC groups. In the top 50 genes, boxed genes are associated with either fibrosis or osteoblast differentiation pathways. (**B**) Gene accessibility tracks of *HOXB* genes (ATAC-seq) show a statistically significant increased accessibility in F-MPN (example of the *HOXB-AS3-HOXB7* region is quantified in the right panel). P-value * - 0.02 calculated using unpaired t test. (**C**) qRT-PCR validation of the ATAC-seq and RNA-seq findings in control (n=13) and F-MPN (n=10) samples. Several *HOXB* genes

are upregulated in F-MPN MSCs. p-values (*- 0.05, **<0.01, ***<0.001) were calculated using unpaired t test. (**D**) In vitro co-culture of normal human mesenchymal cells from the HS-5 cell line with either cells or conditioned media from human hematopoietic cell line UT-7 bearing either the wild type *JAK2* gene (WT) or the mutated *JAK2 V617F* gene (VF) or -with TGF-β (10ng/ml). (**E**) After 7 days co-culture, an increased expression of *HOXB7* and *ACTA2* genes is noted in the MSCs after exposure to TGF-β or *JAK2* mutated cells (VF). p-values (*- 0.05) were calculated using unpaired t test.

Figure 4: Knock-down of *HOXB7* gene alters the potential of MSCs for osteo-differentiation. (**A**) Knock-down of *HOXB7* by shRNA in the HS-5 mesenchymal cell line. The reduced expression of *HOXB7* is validated in an shRNA-transfected cell line by RT-qPCR (left panel). (**B**) Knock-down of *HOXB7* by shRNA in the HS-5 mesenchymal cell line - Western Blot showing absence of HOXB7 in two shRNA transfected cell lines results in down regulation of the downstream target α-SMA (protein encoded by the *ACTA2* gene). (**C**) Gene accessibility tracks of 2 osteoblast-associated genes *ACTA2* and *TAGLN* by ATAC-seq. HS-5 cells with reduced expression of *HOXB7* (HOXB7-KD3) show reduced chromatin accessibility of the *ACTA2* and *TAGLN* genes even after incubation with TGF-β (10ng/ml for 3 days). (**D**) RT-qPCR validation of the ATAC-seq findings showing significant reduced expression of the *ACTA2* and *TAGLN* genes in the *HOXB7* KD3 cells in the presence of TGF-β. p-values *<0.05, **<0.02 calculated using unpaired t test. **(E)** RT q-PCR results showing the downregulation of *HOXB7* and *TAGLN* even in the presence of TGF-β upon DOX addition and the same is restore when the DOX is withdrawn from the same cells after 3 days (n=3). (**F**) Osteoblast differentiation induction assay of HS-5 cells after transfection with either scramble (SCR), *HOXB7* shRNA (*HOXB7* KD 3) alone or after treatment with TGF-β for 21 days. (left panel: microscopy images after osteoblast lineage staining; right panel : arbitrary quantification of osteoblast differentiation). Absence of *HOXB7* reduces osteoblast differentiation even in the presence of TGF-β. p-values were calculated using one way ANNOVA test.

Figure 5: TGF-β induced WNT signaling drives the HOXB7-mediated pro-osteogenic profile of MSCs. (**A**) Treatment of normal human mesenchymal cells (HS-5) with TGF-β (2 and 10 ng/ml) stabilizes β-Catenin levels (immunoblot). (**B**) Treatment of normal human mesenchymal cells (HS-5) with TGF-β (10 ng/ml) induces translocation of β-Catenin to the nucleus (red arrows). Microscopy images after staining with mAb-β-Catenin-(green) and DAPI (blue nucleus) (representative of 3 experiments). (**C**) Chromatin Immunoprecipitation (ChIP) assay of the *HOXB7* promoter. Incubation with TGF-β (10ng/ml) drives an increase in chromatin accessibility (reduction of H3K9me3 marks) and increased binding of β-Catenin (n= 3) to the *HOXB7* promoter. p-value *- 0.02 calculated using unpaired t test. (**D**) Knock-down of β-Catenin in HS-5 cell line by a β-catenin shRNA (β-Cat KD), validated by Western blot (right panel), induces a reduced expression of HOXB7 and its downstream target a-SMA (protein encoded by the *ACTA2* gene) whether in the absence or presence of TGF-β. (**E**) Osteoblast and adipocyte differentiation induction assay of normal mesenchymal HS-5 cells after transfection with either scramble (SCR) or β-Catenin shRNA (β-Cat KD). Microscopy images after respective lineage staining show that absence of B-Catenin decreases osteoblast differentiation and increases adipocyte differentiation. (**F**) Pre-Treatment of HS-5 cells with WNT inhibitor (Cardamonin - 20uM) followed by treatment with TGF-β reduces the expression of HOXB7 and a-SMA along with other WNT pathway genes such as c-MYC and Cyclin-D1 (n=3). (**G**) Treatment of HS-5

cells with TGF-β and WNT inhibitor (Cardamonin -20uM) reduced the expression of *ACTA2* and *TAGLN* genes validated by qRT-PCR assays (n=3). p-value *- 0.02 calculated using unpaired t test. (**H**) Osteo-differentiation induction of HS-5 cells shows a decreased osteoblast differentiation profile upon treatment by cardamonin (20uM) (n=3).

Figure 6: Graphical diagram describing the role of the Wnt/ TGF-β /HOXB7 axis in MPN patients' MSC deregulation. (Illustration created using BioRender).

Figure 1

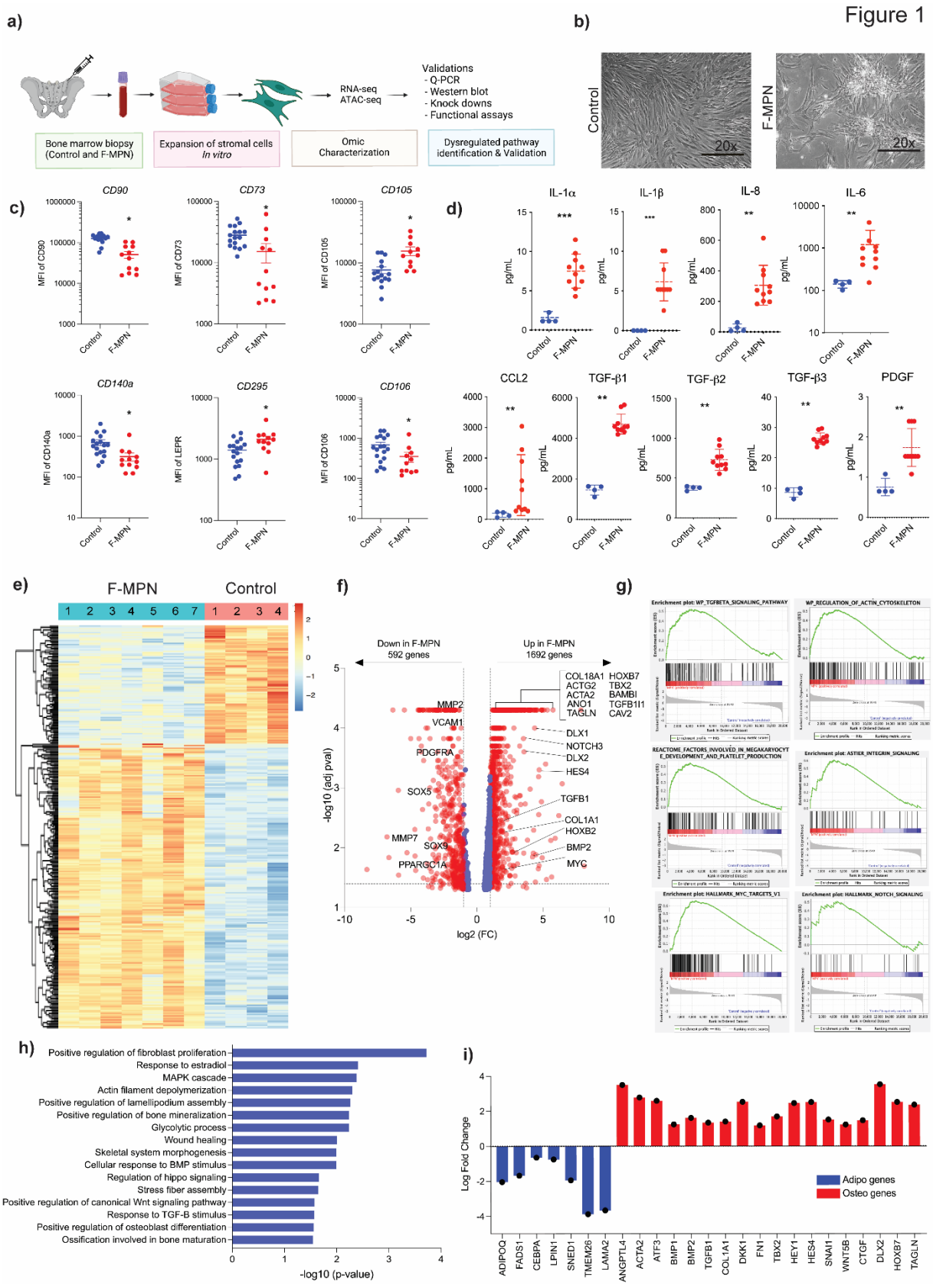
a)
Bone marrow biopsy (Control and F-MPN)
Expansion of stromal cells In vitro
Omic Characterization
RNA-seq ATAC-seq
Validations
- Q-PCR
- Western blot
- Knock downs
- Functional assays
Dysregulated pathway identification & Validation
b)
Control
F-MPN
20x
c)
CD90
CD73
CD105
CD140a
CD295
CD106
MFI of CD90
MFI of CD73
MFI of CD105
MFI of CD140a
MFI of LEPR
MFI of CD106
Control
F-MPN
d)
IL-1α
IL-1β
IL-8
IL-6
CCL2
TGF-β1
TGF-β2
TGF-β3
PDGF
pg/mL
e)
F-MPN
Control
f)
Down in F-MPN 592 genes
Up in F-MPN 1692 genes
-log10 (adj pval)
log2 (FC)
MMP2
VCAM1
PDGFRA
SOX5
MMP7
SOX9
PPARGC1A
COL18A1
ACTG2
ACTA2
ANO1
TAGLN
HOXB7
TBX2
BAMBI
TGFB1I1
CAV2
DLX1
NOTCH3
DLX2
HES4
TGFB1
COL1A1
HOXB2
BMP2
MYC
g)
Enrichment plot: WP_TGFBETA_SIGNALING_PATHWAY
WP_REGULATION_OF_ACTIN_CYTOSKELETON
REACTOME_FACTORS_INVOLVED_IN_MEGAKARYOCYTE_DEVELOPMENT_AND_PLATELET_PRODUCTION
Enrichment plot: ASTIER_INTEGRIN_SIGNALING
Enrichment plot: HALLMARK_MYC_TARGETS_V1
Enrichment plot: HALLMARK_NOTCH_SIGNALING
h)
Positive regulation of fibroblast proliferation
Response to estradiol
MAPK cascade
Actin filament depolymerization
Positive regulation of lamellipodium assembly
Positive regulation of bone mineralization
Glycolytic process
Wound healing
Skeletal system morphogenesis
Cellular response to BMP stimulus
Regulation of hippo signaling
Stress fiber assembly
Positive regulation of canonical Wnt signaling pathway
Response to TGF-B stimulus
Positive regulation of osteoblast differentiation
Ossification involved in bone maturation
-log10 (p-value)
i)
Log Fold Change
Adipo genes
Osteo genes
ADIPOQ
FADS1
CEBPA
LPIN1
SNED1
TMEM26
LAMA2
ANGPTL4
ACTA2
ATF3
BMP1
BMP2
TGFB1
COL1A1
DKK1
FN1
TBX2
HEY1
HES4
SNAI1
WNT5B
CTGF
DLX2
HOXB7
TAGLN

Figure 2

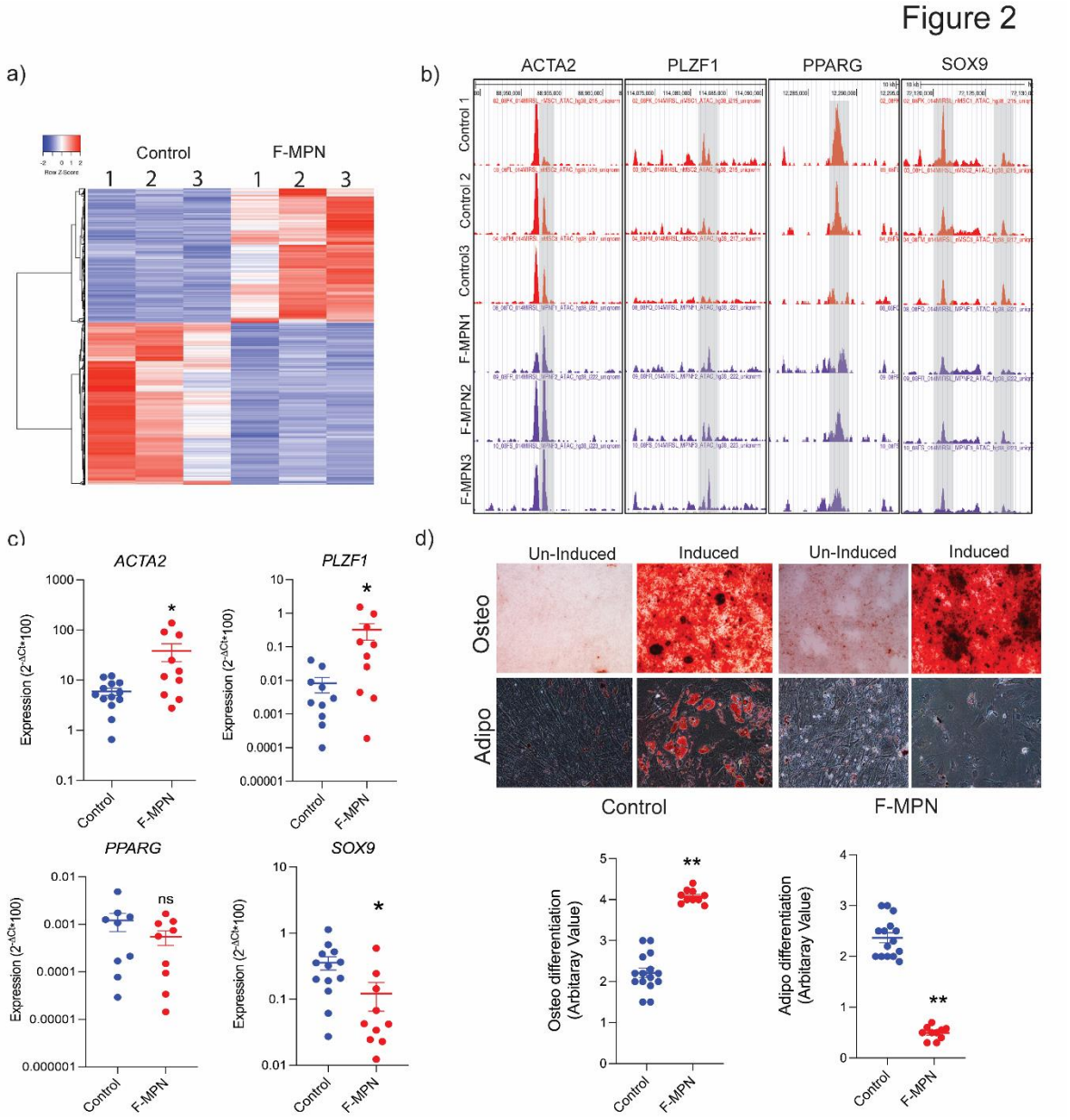
a)
Control
F-MPN
1 2 3 1 2 3
b)
ACTA2
PLZF1
PPARG
SOX9
Control 1
Control 2
Control3
F-MPN1
F-MPN2
F-MPN3
c)
ACTA2
PLZF1
PPARG
SOX9
Expression (2-ΔCt*100)
Control
F-MPN
ns
*
d)
Un-Induced
Induced
Un-Induced
Induced
Osteo
Adipo
Control
F-MPN
Osteo differentiation (Arbitaray Value)
Adipo differentiation (Arbitaray Value)
**

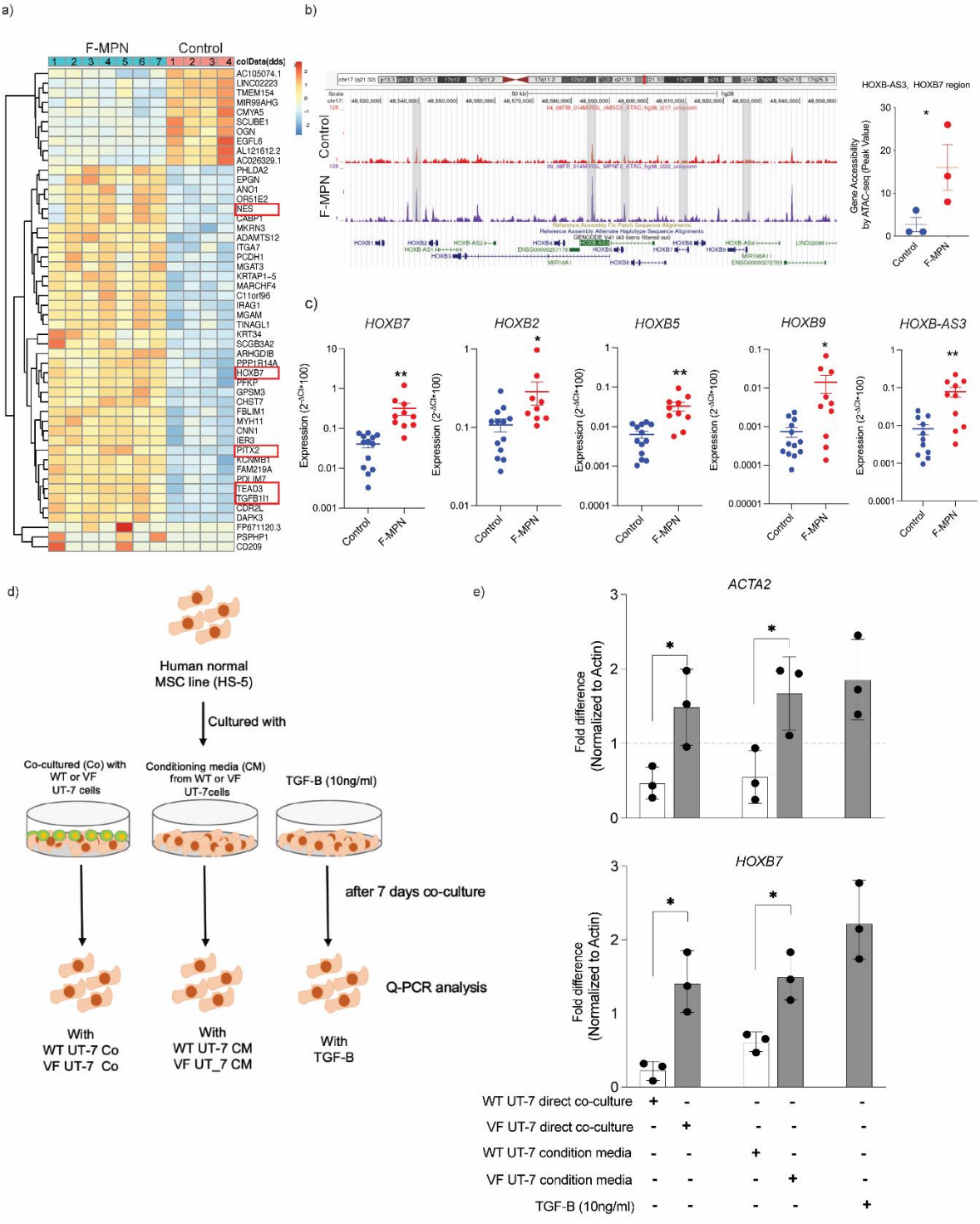
a)
F-MPN
Control
colData(dds)
AC105074.1
LINC02223
TMEM154
MIR99AHG
CMYA5
SCUBE1
OGN
EGFL6
AL121612.2
AC026329.1
PHLDA2
EPGN
ANO1
OR51E2
NES
CABP1
MKRN3
ADAMTS12
ITGA7
PCDH1
MGAT3
KRTAP1–5
MARCHF4
C11orf96
IRAG1
MGAM
TINAGL1
KRT34
SCGB3A2
ARHGDIB
PPP1R14A
HOXB7
PFKP
GPSM3
CHST7
FBLIM1
MYH11
CNN1
IER3
PITX2
KCNMB1
FAM219A
PDLIM7
TEAD3
TGFB1I1
CDR2L
DAPK3
FP671120.3
PSPHP1
CD209
b)
Control
F-MPN
HOXB-AS3, HOXB7 region
Gene Accessibility by ATAC-seq (Peak Value)
Control
F-MPN
c)
HOXB7
HOXB2
HOXB5
HOXB9
HOXB-AS3
Expression (2^-ΔCt*100)
Control
F-MPN
d)
Human normal MSC line (HS-5)
Cultured with
Co-cultured (Co) with WT or VF UT-7 cells
Conditioning media (CM) from WT or VF UT-7cells
TGF-B (10ng/ml)
after 7 days co-culture
Q-PCR analysis
With WT UT-7 Co VF UT-7 Co
With WT UT-7 CM VF UT_7 CM
With TGF-B
e)
ACTA2
HOXB7
Fold difference (Normalized to Actin)
WT UT-7 direct co-culture
VF UT-7 direct co-culture
WT UT-7 condition media
VF UT-7 condition media
TGF-B (10ng/ml)

Figure 4

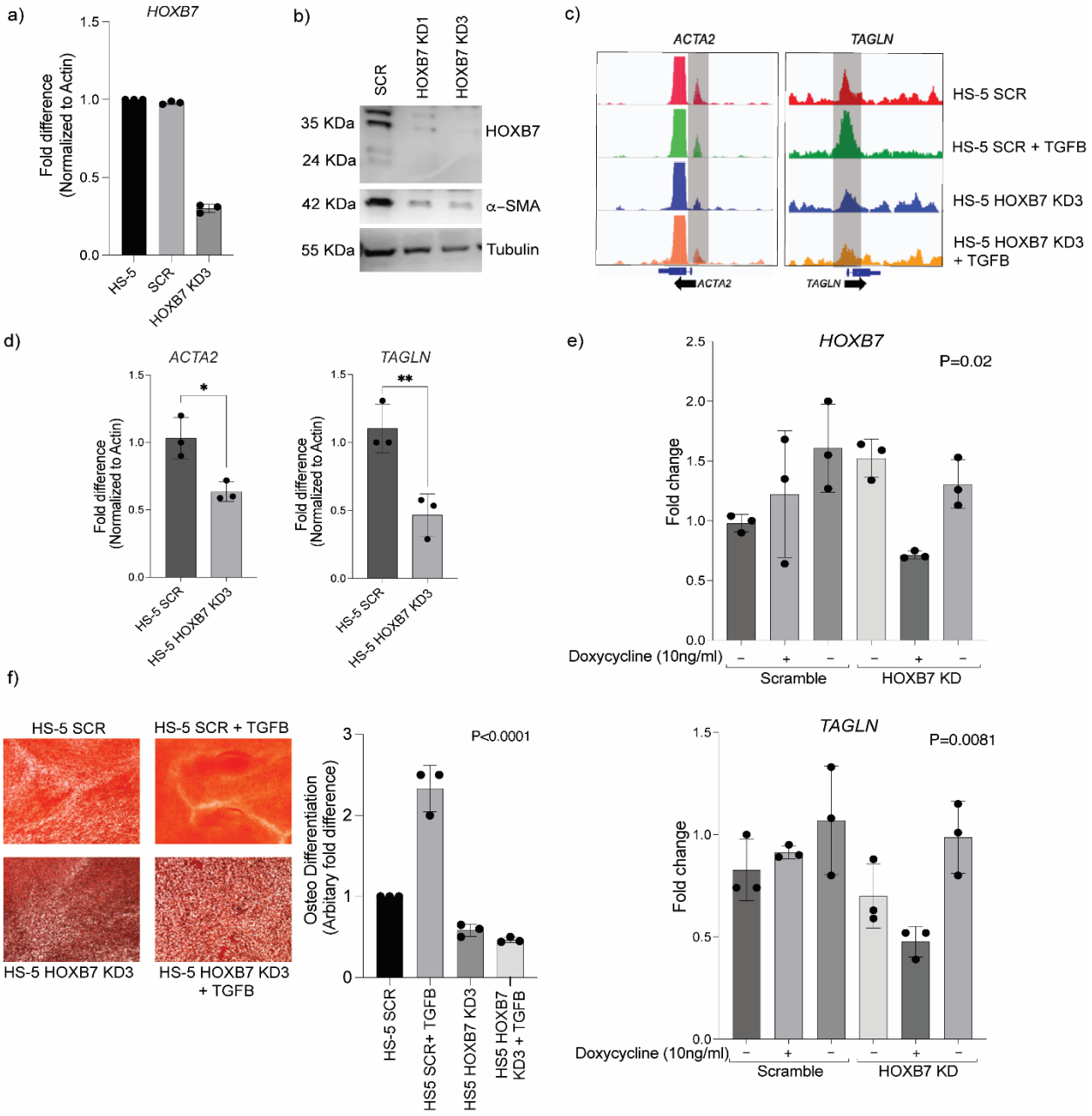
a)
HOXB7
Fold difference (Normalized to Actin)
1.5
1.0
0.5
0.0
HS-5
SCR
HOXB7 KD3
b)
SCR
HOXB7 KD1
HOXB7 KD3
35 KDa
24 KDa
HOXB7
42 KDa
α–SMA
55 KDa
Tubulin
c)
ACTA2
TAGLN
HS-5 SCR
HS-5 SCR + TGFB
HS-5 HOXB7 KD3
HS-5 HOXB7 KD3 + TGFB
ACTA2
TAGLN
d)
ACTA2
*
Fold difference (Normalized to Actin)
HS-5 SCR
HS-5 HOXB7 KD3
TAGLN
**
Fold difference (Normalized to Actin)
HS-5 SCR
HS-5 HOXB7 KD3
e)
HOXB7
P=0.02
Fold change
2.5
2.0
1.5
1.0
0.5
0.0
Doxycycline (10ng/ml)
– + – – + –
Scramble
HOXB7 KD
f)
HS-5 SCR
HS-5 SCR + TGFB
HS-5 HOXB7 KD3
HS-5 HOXB7 KD3 + TGFB
Osteo Differentiation (Arbitary fold difference)
P<0.0001
3
2
1
0
HS-5 SCR
HS5 SCR+ TGFB
HS5 HOXB7 KD3
HS5 HOXB7 KD3 + TGFB
TAGLN
P=0.0081
Fold change
1.5
1.0
0.5
0.0
Doxycycline (10ng/ml)
– + – – + –
Scramble
HOXB7 KD

Figure 5

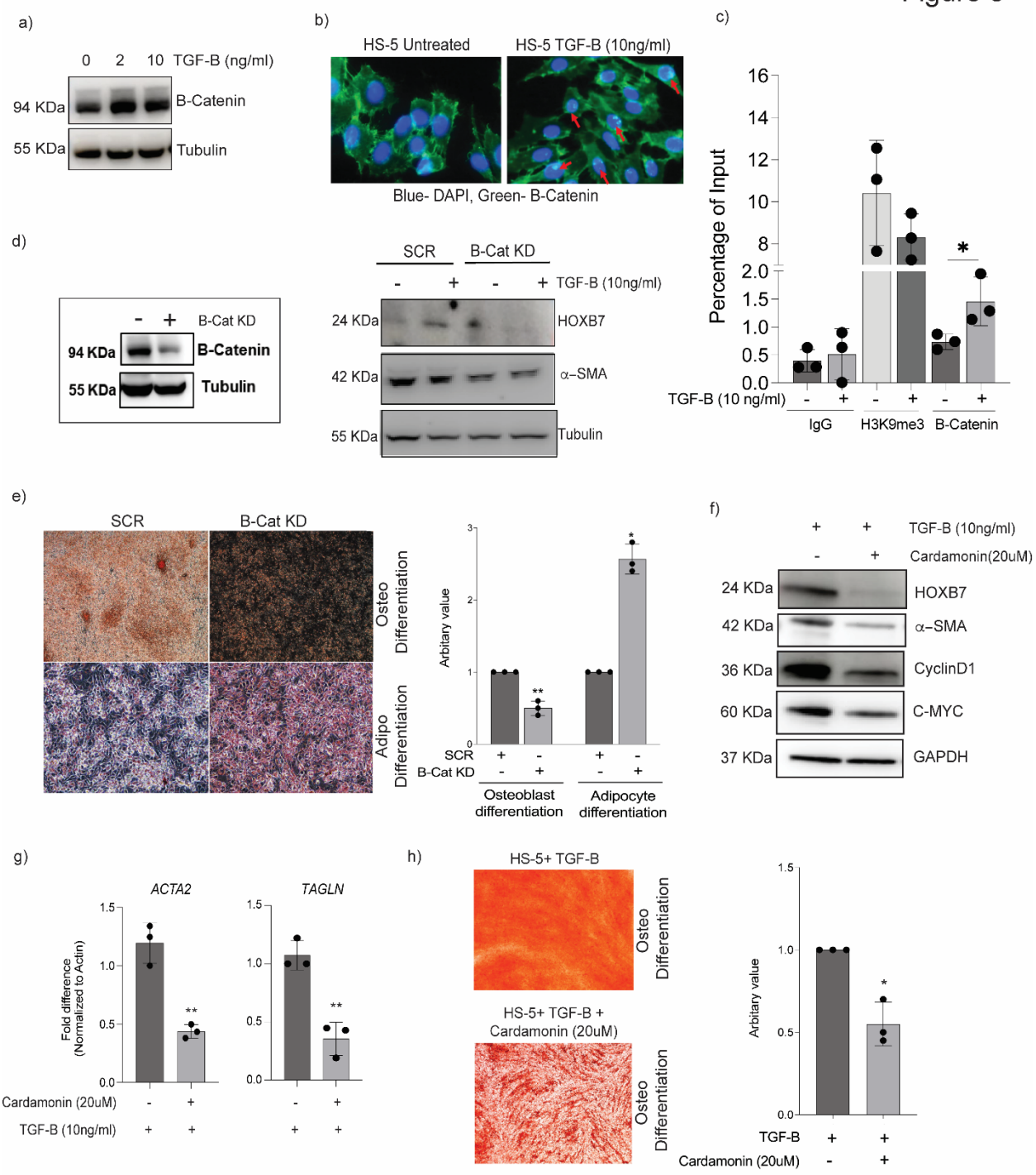
a)
0 2 10 TGF-B (ng/ml)
94 KDa
B-Catenin
55 KDa
Tubulin
b)
HS-5 Untreated
HS-5 TGF-B (10ng/ml)
Blue- DAPI, Green- B-Catenin
c)
Percentage of Input
TGF-B (10 ng/ml)
IgG
H3K9me3
B-Catenin
d)
B-Cat KD
94 KDa
B-Catenin
55 KDa
Tubulin
SCR
B-Cat KD
TGF-B (10ng/ml)
24 KDa
HOXB7
42 KDa
α–SMA
55 KDa
Tubulin
e)
SCR
B-Cat KD
Osteo Differentiation
Adipo Differentiation
Arbitary value
SCR
B-Cat KD
Osteoblast differentiation
Adipocyte differentiation
f)
TGF-B (10ng/ml)
Cardamonin(20uM)
24 KDa
HOXB7
42 KDa
α–SMA
36 KDa
CyclinD1
60 KDa
C-MYC
37 KDa
GAPDH
g)
ACTA2
TAGLN
Fold difference (Normalized to Actin)
Cardamonin (20uM)
TGF-B (10ng/ml)
h)
HS-5+ TGF-B
HS-5+ TGF-B + Cardamonin (20uM)
Osteo Differentiation
Arbitary value
TGF-B
Cardamonin (20uM)

Figure 6

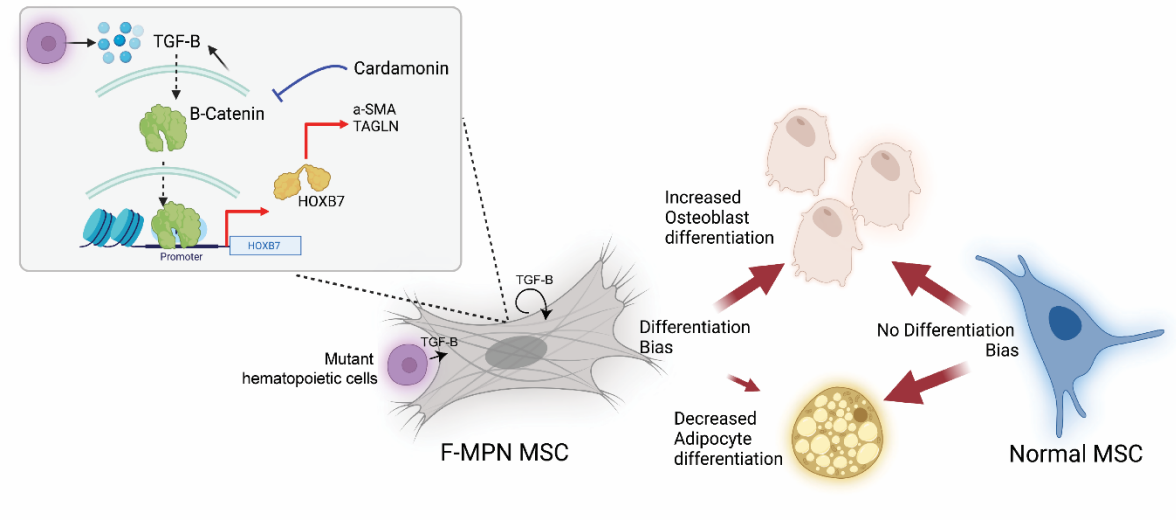
TGF-B
Cardamonin
B-Catenin
a-SMA
TAGLN
HOXB7
Promoter
HOXB7
TGF-B
TGF-B
Mutant
hematopoietic cells
F-MPN MSC
Increased
Osteoblast
differentiation
Differentiation
Bias
No Differentiation
Bias
Decreased
Adipocyte
differentiation
Normal MSC